



# High-Performance Enhancement of a GaAs Photodetector Using a Plasmonic Grating

Bedir Yousif<sup>1</sup> · Mohy Eldin A. Abo-Elsoud<sup>2</sup> · Hagar Marouf<sup>3</sup>

Received: 22 November 2019 / Accepted: 17 February 2020 / Published online: 8 April 2020  
© Springer Science+Business Media, LLC, part of Springer Nature 2020

## Abstract

In this study, we present and establish a gold surface plasmon polariton (SPP) GaAs photodetector that achieves high internal quantum efficiency (IQE). At a wavelength of 600 nm, the IQE with the SPP was 85%, while the IQE without the SPP was 42%, an enhancement of 43%. Also, at a wavelength of 675 nm, the IQE with SPP was 82%, whereas the IQE without SPP was 45%, which constitutes an increase of 37%. Such excellent performance is ascribed to the subwavelength scope of the optical power in the photoconductive-based gold SPP GaAs that provides high IQE. Moreover, the recombination of the SPP in the photodetector provides greater photocurrent and responsivity.

**Keywords** Plasmonic photodetectors · Surface plasmon polaritons · Light trapping · GaAs photodetector · Plasmonic grating

## Introduction

Plasmonic photodetectors have attracted great interest in the field of photonics in recent decades. Plasmonics is desirable as metal structures are capable of trapping light by coupling an electromagnetic wave with charged carrier oscillations at the metal surface. The wavelength of these oscillations is significantly smaller than that of the corresponding wavelength of light in space, which enables subwavelength-scale light–matter interaction, thus enabling the design of ultra-compact devices with the potential for higher speed. The integration of surface plasmon polariton (SPP) technology in the fabrication of photodetectors has shown great promise in the development of active GaAs PIN circuits. By exploiting the ability of metals to constrain light at the deep-

subwavelength scale, plasmonics has enabled a substantial reduction in the size of photonic components [1–8], advancing the technology toward the scaled combination of electronic and optical components [8]. This paves the way for the next generation of ultra-dense interconnects [9] with integrated optoelectronic interfaces. Furthermore, the realization of high-speed devices [10–12] will help to fulfill the growing demand for ultrafast detection in both the communications and sensing markets (<http://www.ethemetalliance.org/roadmap/>), i.e., for decoding of high-speed optical signals and for high-speed detection, respectively [13]. Metal components are an inherent feature of plasmonic photodetectors. Different categories of plasmonic photodetectors are shown in Fig. 1.

In modeling, a gallium arsenide (GaAs) semiconductor is commonly used as the substrate. GaAs is preferred for the design of electronic and photonic devices because of its unique electrical and optical characteristics as a compound semiconductor (Cha, 2004). The GaAs substrate offers a wide range of bandwidth and good responsivity because of its short absorption length. Because it is a direct-bandgap semiconductor, it can collect and produce light more efficiently than an indirect-bandgap semiconductor. GaAs has a conduction-band construction which leads to high-speed electron conduction.

Surface plasmon polaritons (SPPs), which travel along a metal–dielectric interface, are excitations that occur as a result of the coupling of the light and collective oscillations of free electrons [4, 14–16]. In low-frequency domains where SPPs do not exist naturally, spoof SPPs on nanostructured metals can find a number of intriguing applications [3, 17–19].

✉ Hagar Marouf  
hagamarouf9999@gmail.com

Bedir Yousif  
bedir.yousif@eng.kfs.edu.eg; bedir.yousif@gmail.com

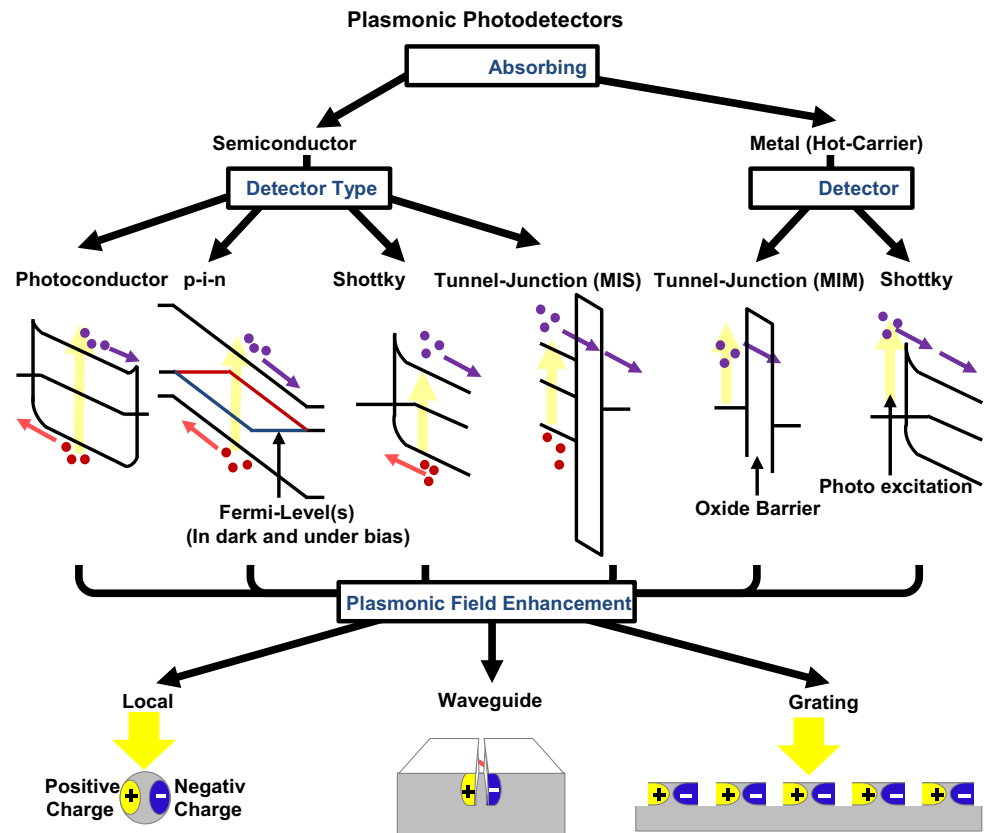
Mohy Eldin A. Abo-Elsoud  
2-mohyldin@gmail.com; mohyldin@ieee.org

<sup>1</sup> Electrical Engineering Department, Faculty of Engineering, Kafrelsheikh University, Kafrelsheikh 35514, Egypt

<sup>2</sup> Electronics and Communications Department, Faculty of Engineering, Mansoura University, Mansoura 35516, Egypt

<sup>3</sup> Electronics and Communications Department, Delta High Institute for Engineering and Technology, Delta Academy, Damietta 34511, Egypt

**Fig. 1** Summary of types of plasmonic photodetectors. These detectors can be improved by plasmonics via a local, waveguide, or grating methodology



Despite the improvements and advancements in SPP technology, the efficient and unidirectional SPP excitation remains one of the greatest challenges because of the fundamental momentum mismatch between the propagating waves and surface waves that prevents their direct coupling. A specific potential gradient is able to be subjectively manipulated by adjusting the electric field, substantially improving the device performance beyond conventional bandgap engineering [20]. Because they can be size-scaled to operate across the entire electromagnetic spectrum, structured plasmonic metamaterials provide a new pathway for the design of functionalized optical and electrical components. Furthermore, the high conduction electron density offers an opportunity to extend plasmon energy in the near-visible range [21].

In this paper, we utilize a plasmonic grating at the surface of the model that is very useful for controlling the absorbed light, manipulating and detecting light with specific polarization. The plasmonic grating leads to enhanced absorption and demonstrates excellent performance in reducing losses and allowing the propagation of light power in the optoelectronic devices.

Here, we used a tool box on a PIN photodetector. The study involved adding gold surface plasmon polaritons (SPPs) at the top of the PIN photodetector, which also revealed its influence in increasing the photocurrent, internal quantum efficiency (IQE), spectral response and responsivity.

The remainder of the paper is structured as follows: Section 2 presents the structure of our PIN photodetector model and the parameters values. Section 3 explains the mathematical modeling of the SPP used in this research. The results of the simulation are explained in Section 4. Lastly, Section 5 provides a summary and conclusions of this study.

## Model Structure

In this section, we discuss the model structure of the improved PIN photodetector. As shown in Fig. 2, the GaAs PIN photodetector was simulated using gold as the SPP layer on the surface of the photodetector. We chose blown GaAs with 1  $\mu\text{m}$  thickness as active material. The gold SPP layer was constructed at the top of the model, and the P connector and N connector were made of silver to detect the current flow throughout the photodetector as soon as the light condition was induced. Additional information regarding the model is provided in Table 1.

## Mathematical Modeling of the SPP

### Excitation of the SPP

SPPs can be excited by both photons and electrons. The excitation by electrons is generated by exciting electrons into the

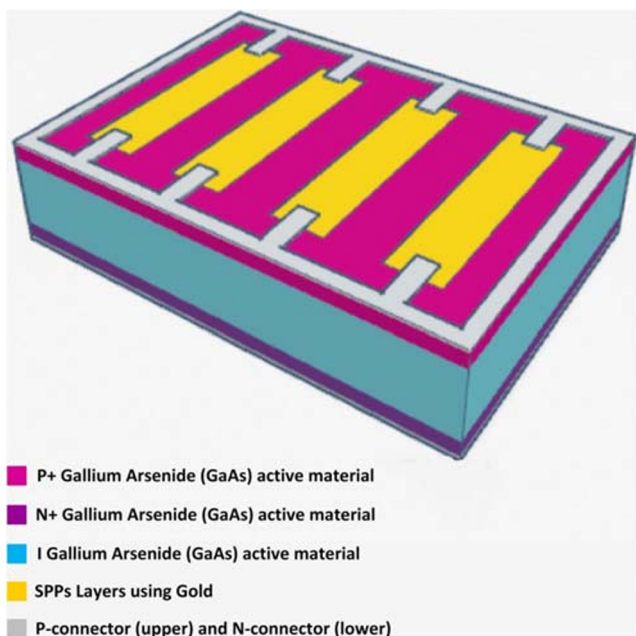


Fig. 2 Gallium arsenide (GaAs) PIN photodetector with gold SPP layer

bulk of the metal. As the electrons are scattered, the light energy is transferred into the plasma form [22].

In order for a photon to excite an SPP, both must have the same frequency and momentum. However, for any given frequency, a free-space photon has greater momentum than the SPP because they have different dispersion relations. This prevents the direct coupling of a free-space photon in air with an SPP. Similarly, an SPP on a smooth metal surface cannot emit energy as a free-space photon into the dielectric. This is the same phenomenon seen with the lack of transmission that occurs through reflection. The excitation wavelength of the SPPs is:

$$\lambda_{SPP} = \frac{2\pi}{K_x} \approx \sqrt{\frac{\epsilon_1 + \epsilon_2}{\epsilon_1 \epsilon_2}} \lambda \tag{1}$$

where  $\lambda$  the wavelength of the excitation light in space. This dampening is produced by ohmic losses of the electrons

Table 1 Model parameters

Parameter	Parameter value
Incident power	1000 [W/m <sup>2</sup> ]
N-contact voltage	2 [V]
P-contact voltage	0 [V]
Refractive index of GaAs (real component)	3.5
Detector thickness	1 [μm]
Anode doping (P+ doping)	1e21 [atom/cm <sup>3</sup> ]
Anode doping thickness	100 [nm]
Cathode doping (N+ doping)	1e21 [atom/cm <sup>3</sup> ]
Cathode doping thickness	100 [nm]
SPP layer width	500 [nm]
SPP layer thickness	3.7 [nm]
Distance between two SPP layers	500 [nm]

contributing in the SPP, which results in heating the metal. Using  $\epsilon_2 = 1$  and the dielectric function of gold ( $\epsilon_1 = -11.6 + 1.2i$ ), at a wavelength of 623 nm, we get 1/e intensity propagation lengths for the SPP of 60 μm and 10 μm, respectively [16, 23].

### The Fields and Dispersion Relation in SPP

The characteristics of the SPP can be obtained using Maxwell’s equations. We utilize a coordinate scheme where the metal–dielectric interface is the  $Z = 0$  plane, with the metal at  $Z < 0$  and the dielectric at  $Z > 0$ . The electric and magnetic fields as a function of position  $(x, y, z)$  and time  $t$  are as follows [24, 25].

$$E_{x,n}(x, y, z, t) = E_0 e^{ik_x x + ik_{z,n} |z| - i\omega t} \tag{2}$$

$$E_{z,n}(x, y, z, t) = \pm E_0 \frac{k_z}{k_{z,n}} e^{ik_x x + ik_{z,n} |z| - i\omega t} \tag{3}$$

$$H_{y,n}(x, y, z, t) = H_0 e^{ik_x x + ik_{z,n} |z| - i\omega t} \tag{4}$$

where

- $n$  denotes the physical material (1 for the metal at  $z < 0$  or 2 for the dielectric at  $z > 0$ ).
- $\omega$  is the angular frequency of the waves.
- The  $\pm$  is + for the metal and – for the dielectric.
- $E_x, E_z$  are the  $x$  and  $z$  components for the electric field vector,  $H_y$  is the  $y$  component for the magnetic field vector, and the other components ( $E_x, E_y, H_y$ ) are zero. SPPs are always transverse magnetic (TM) waves.
- $K$  is the wave vector. It is a complex vector. In the case of a lossless SPP, it turns out that the  $x$  components are real and the  $z$  components are imaginary. The wave oscillates along the  $x$  direction and exponentially decreases along the  $z$  direction.  $k_x$  is always the same for both materials, but  $k_{z,1}$  is generally different from  $k_{z,2}$ .
- $\frac{H_0}{E_0} = -\frac{\epsilon_1 \omega}{k_{z,1} c}$ , where  $\epsilon_1$  is the permittivity of the metal. We can write it as  $\frac{H_0}{E_0} = -\frac{\epsilon_2 \omega}{k_{z,2} c}$

A wave of this form satisfies Maxwell’s equations only on condition that the following equations also hold:

$$\frac{k_{z,1}}{\epsilon_1} + \frac{k_{z,2}}{\epsilon_2} = 0 \tag{5}$$

and

$$K^2_x + K^2_{zn} = \epsilon_n \left(\frac{\omega}{c}\right)^2 \quad n=1,2 \tag{6}$$

Solving these two equations, we obtain the dispersion relation for a wave propagating on the surface as

$$k_z = \frac{w}{C} \left( \frac{\varepsilon_1 \varepsilon_2}{\varepsilon_1 + \varepsilon_2} \right)^{1/2} \quad (7)$$

In the free-electron model of the electron gas, which neglects attenuation, the metal dielectric function is obtained as [26]:

$$\varepsilon(w) = 1 - \frac{w_p^2}{w^2} \quad (8)$$

where the bulk plasma frequency in SI units is

$$w_p = \sqrt{\frac{ne^2}{\varepsilon_0 m^*}} \quad (9)$$

where  $n$  is the electron density,  $e$  is the charge of the electron,  $m^*$  is the effective mass of the electron and  $\varepsilon_0$  is the permittivity of free space. At low  $k$ , the SPP acts as a photon, but as  $k$  increases, the dispersion relation bends and reaches an asymptotic limit referred to as the “surface plasma frequency”.

Similar to the metal-SPP, it can be considered that the surface wave for metal–dielectric multilayers is also created by the coupling between the electromagnetic field and the electronic fluctuation [27]. Such a wave is confined to the boundary of the metamaterial and propagates along the interface. Ordinarily, the electromagnetic field decays exponentially, as the energy is restricted near the boundary and will not propagate inside substantially. As revealed in Fig. 3, the thickness of the plasmon of a blank substrate is dependent on the imaginary part of the dielectric constant of the thin film, and its position is improved by virtue of the thickness of the dielectric layer. As observed from Fig. 3, the dispersion relation changes and the resonance angle is shifted when a thin dielectric layer is adsorbed on the surface of the thin metal film. Such a shift of the resonance angle is proportional to the optical thickness, which is affected by the difference between the refractive indices and the thickness of the thin film.

### Propagation Length and Skin Depth in SPP

As the SPP propagates along the surface, it loses energy to the metal because of absorption. The intensity of the surface plasmon decays in proportion to the square of the electric field; therefore, at a distance  $X$ , the intensity is reduced by a factor of  $\exp\{-2k_x^i X\}$ . The propagation length is defined as the distance for the SPP energy to decay by a factor of  $1/e$ , which is satisfied at a length [28].

$$L = \frac{1}{2k_x^i} \quad (10)$$

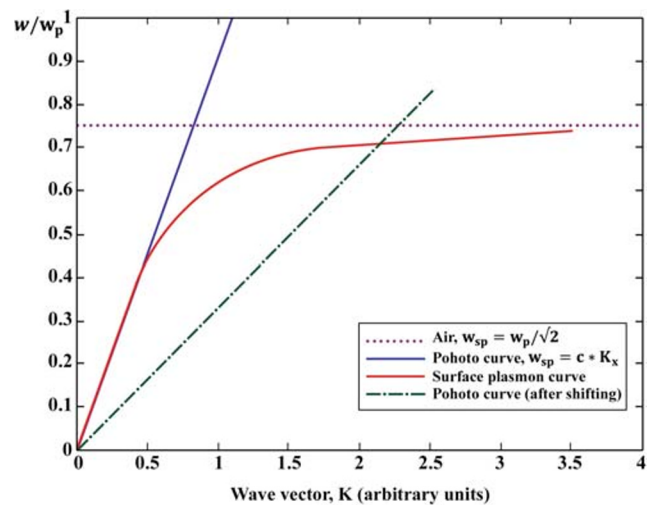


**Fig. 3** Dispersion relation of the surface plasmon with the photon. As  $k$  increases, the dispersion curve bends downward and reaches the asymptotic limit

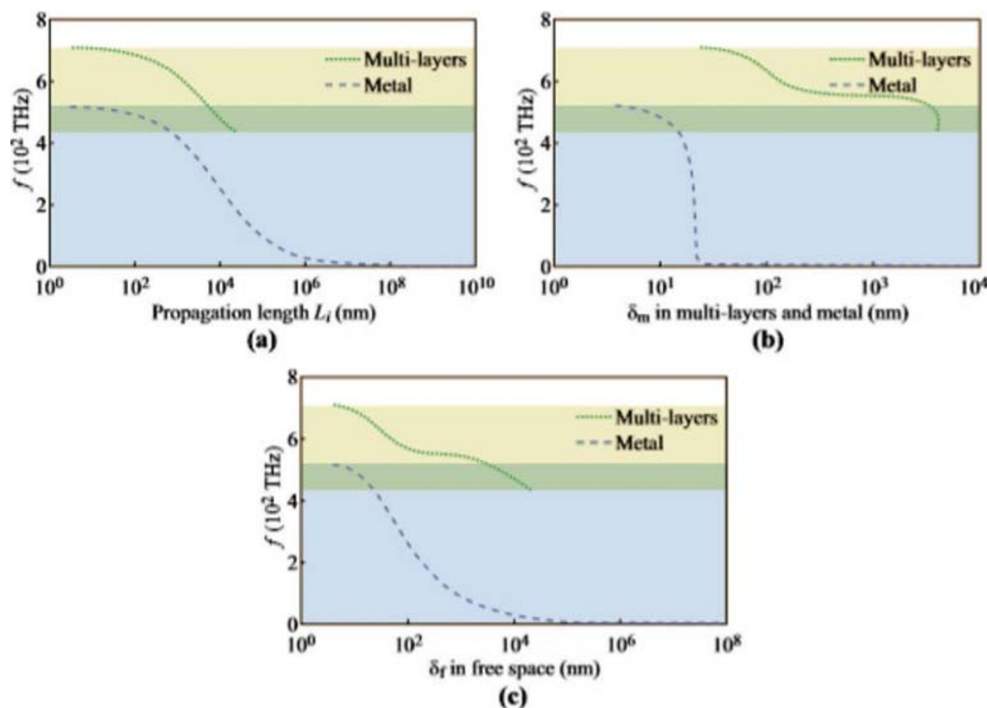
Similarly, the electric field decreases evanescently perpendicularly to the metal surface. At low frequencies, the depth of SPP penetration into the metal is typically estimated via the skin depth formula. In the dielectric, the electric field will decrease more gradually. The length of the decay in the metal and dielectric medium can be expressed as [29]:

$$Z_i = \frac{\lambda}{2\pi} \left( \frac{|\varepsilon_1 + \varepsilon_2|}{\varepsilon_i^2} \right)^{1/2} \quad (11)$$

where  $i$  is the propagation medium. SPPs are very sensitive to small disturbances in the skin depth; as a result, SPPs are frequently utilized to investigate inhomogeneities of a surface.

Figure 4 shows the frequency range of the multilayer-SPPs (light green part) and that of the metal-SPP (light blue part). It is clear that the frequency range of the multilayer-SPP is higher and narrower than that of the metal. We know that the surface plasmon is caused by the oscillation of free electrons at metal surface. Thus a reduction in the number of free electrons would lead to a decrease in the frequency range, because the negativity of  $\varepsilon_m$  is positively related to the concentration of free electrons. In most instances, the metal with lower free electron density exhibits a lower  $w_{sp}$ , which indicates the upper bound of the frequency range. Here, the lower  $w_{sp}$  occurs because the multilayers with lower free electron density replacesome parts of the metal with dielectric layers. However, this cannot be true, because the calculation indicates that this structure is capable of extending the SPP to a higher frequency where even metal-SPP cannot exist. Figure 4 shows the above characteristic length of each metal-SPP and multilayer-SPP. It is obvious that the propagation length of the multilayer-SPPs is around five times greater than that of the metal-SPP at the same frequency. Therefore, the propagation loss is much lower for the multilayer-SPPs than the metal SPP.

**Fig. 4** The (a) propagation length, (b) skin depth in multi-layers and (c) skin depth in free space of the metal-SPP and multilayer-SPP. The light green and light blue colors indicate the frequency range of the multilayer-SPPs besides the metal-SPP, correspondingly



The reason for this is that more of the multilayer-SPP field increases inside the dielectric area ( $Z > 0$ ) (Fig. 4c) and also occurs in the dielectric parts of the multilayer structure ( $Z < 0$ ) (Fig. 4b). Consequently, in such conditions, replacing the original metal with a multilayer structure would cause the propagation length to increase. The properties of the SPP could then be tuned by adjusting the metal/dielectric ratio of the multilayers.

### Operational Parameters of the PIN Photodetector

We can calculate the internal quantum efficiency (IQE) using [30]:

$$IQE = \frac{I_p}{P_{in}} \cdot \frac{hc}{\lambda \cdot e} \tag{12}$$

The responsivity (R) is the ratio between the photocurrent ( $I_p$ ) and the input power ( $P_{in}$ ) calculated as follows [31]:

$$R = \frac{I_p}{P_{in}} \tag{13}$$

We can define the photocurrent as [32].

$$(I_p) = IQE \cdot e \left( \frac{P_{opt}}{h \cdot \nu} \right) \tag{14}$$

where  $e$  is the elementary charge,  $P_{opt}$  is the optical power, and  $h$  is the Planck constant. Photocurrent can be described as an

electric current that is generated by means of incident light in a photodetector [33].

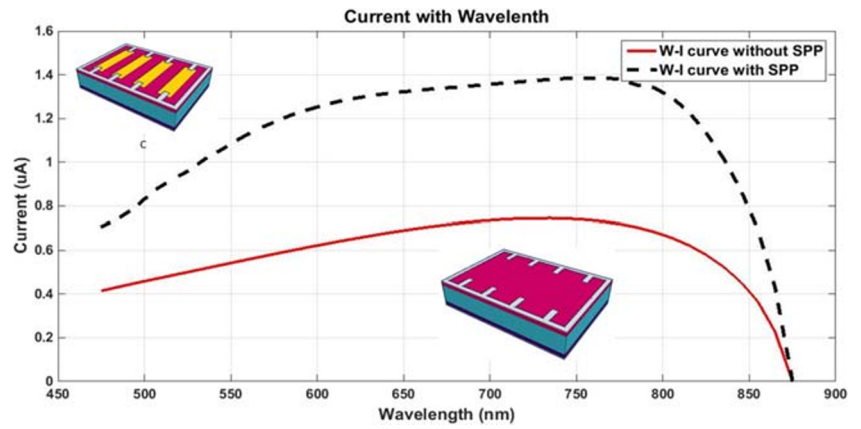
In most cases, one obtains at most one photoelectron per absorbed photon. Some of the carriers generated may contribute only weakly to the photocurrent and thus be lost, which is calculated by the quantum efficiency, for example, of a photodiode. Even in photovoltaic mode, i.e., with zero bias voltage, the quantum efficiency is not greatly reduced, and some forward voltage is required to significantly decrease the photocurrent. Therefore, the bias voltage frequently has only a slight influence on the responsivity. For many detectors, the photocurrent is nearly exactly proportional to the incident optical intensity or power over many decades until a specific level of saturation is achieved [34, 34].

Absorption can be expressed as follows: when the energy of a photon is equal to or greater than the bandgap of the material, the photon is attracted by the material and excites an electron into the conduction band.

Photons incident on the surface of a semiconductor will be either reflected from the upper surface or absorbed into the material, or, failing both of these processes, will be transmitted across the material. For photovoltaic devices, reflection and transmission are generally considered loss mechanisms, as photons that are not absorbed do not produce power. If the photon is absorbed, it has the potential to excite an electron from the valence band into the conduction band [36].

The absorption coefficient is dependent both on the material and on the wavelength of light that is being absorbed. Semiconductor materials have a sharp edge in their absorption

**Fig. 5** Current as a function of photodetector position (nm) for a range of wavelengths. The simulation was carried out under the following conditions: gallium arsenide doping  $1 \times 10^{21}$  atoms/cm<sup>3</sup>,  $\lambda$  of 675 nm, and voltage bias 2 V



coefficient, since light that has energy below the bandgap does not have sufficient energy to excite an electron into the conduction band from the valence band.

For a perfect absorber with unity absorption **A**, we need reduce both the transmission **T** and reflectivity **R**; that is, **A = 1 - R - T**.

Transmission is easily decreased with the use of a metallic back plate. The reflectivity of an incident electromagnetic wave normal to a metamaterial absorber is expressed as follows [37].

$$R = \left| \frac{Z(\omega) - Z_0(\omega)}{Z(\omega) + Z_0(\omega)} \right|^2 \tag{15}$$

where  $Z(\omega) = \sqrt{\mu(\omega)\mu_0/\varepsilon(\omega)\varepsilon_0}$  is the impedance of the metamaterial absorber and  $Z_0 = \sqrt{\mu_0/\varepsilon_0}$  is the impedance of free space. For reflectivity to be zero, the impedance match condition  $Z(\omega) = Z_0(\omega)$  must be satisfied, and therefore the condition  $\mu(\omega) = \varepsilon(\omega)$  must be met. As there are no natural magnetic materials in the optical regime (i.e.,  $\mu = 1$  for all materials), a metamaterial with a nonunity permeability  $\mu(\omega)$  enables us to obtain perfect absorption at a specific frequency via impedance matching with free space [38]. The reflectivity at a frequency  $\omega$  is:

$$R = \frac{(\omega - \omega_0)^2}{(\omega - \omega_0)^2 + \Gamma^2/4} \tag{16}$$

where  $\Gamma$  and  $\omega_0$  are the resonance width and frequency, respectively. Because the objective is zero reflectivity, it is obvious that this equation will be zero, and hence reflectivity will be zero at a frequency when  $\omega = \omega_0$  [39].

The probability of a photon being absorbed is dependent on the probability of the interaction between a photon and electron in which a transfer from one energy band to another occurs. For photons having energy very close to the bandgap, the absorption is relatively low, because only the electrons at the edge of the valance band can interact with the photon to produce absorption. When the photon energy increases, a greater number of electrons can interact with the photon, and absorption of the photon can occur.

The absorption coefficient  $\alpha$  is correlated with the extinction coefficient  $k$  by the following equation [40]:

$$\alpha = \frac{4\pi k}{\lambda} \tag{17}$$

**Fig. 6** Photocurrent as a function of irradiance. The simulation was implemented under the following conditions: gallium arsenide doping  $1 \times 10^{21}$  atom/cm<sup>3</sup>,  $\lambda$  675 nm, and voltage bias 2 V

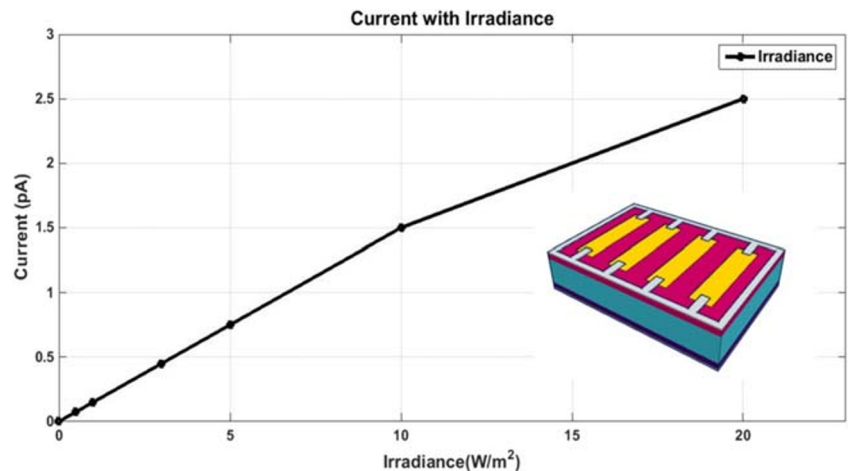
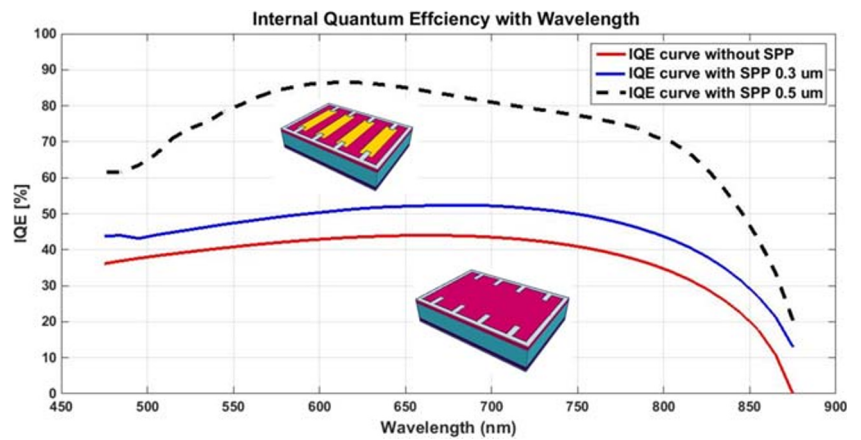


**Fig. 7** Simulated internal quantum efficiency versus wavelength



**Simulation Results**

Many metal nano-sized structures including subwavelength slits have plasmonic effects and can form a region of high light intensity with respect to the light wavelength and the geometry of the nanostructure. The frequencies in the visible spectrum are all absorbed in the bonds and are able to travel through the metal by means of electron transfer because of their empty electron states. With surface illumination, metals reflect almost all the energy with the same incident wavelength, while the absorbed light is emitted by the surrounding free electrons, which gives the metal surface its glossy or shiny appearance. Among these, noble metals have extraordinary features that make them suitable for a wide range of plasmonic applications. For plasmonic interactions to occur, metals with unique characteristics are required. The interaction of light with resonant nanostructures at the interface between the metal and dielectric produces the SPPs. Here, the metal assumes a more substantial role than the dielectric in plasmonic applications, given its distinctive electrical and optical properties arising from the large number of free electrons. The fundamental sign is the construction of metals that are used in plasmonics that are nanostructured metals and not the bulk form. The use of gold SPPs provides excellent

light trapping and better IQE and responsivity. In our paper we reveal a 2-D simulation to reflect the highest significant parameters for the PIN photodetector and show our improvement with gold SPP.

Periodic nanostructures can efficiently generate light transmission and absorption through excitation of surface plasmons (SPs), and their potential for application in optical communication systems has made them an interesting type of device. The typical MSM-PD is a symmetric device consisting of two Schottky diodes connected back-to-back on a semiconductor substrate [4], such as GaAs, which as a direct-bandgap semiconductor collects and emits photons more effectively than indirect semiconductors such as Si and Ge [41].

The SPPs can be effectively excited in the nanostructured noble metals because they practically have free-electron performance. The noble metal nanotextured structures have superior properties to generate localized areas of high energy density and show greater enhancement for extraordinary optical absorption (EOA). This influence and its underlying mechanism have important applications in photolithography and near-field microscopy [42].

The enhanced absorption produced by the excitation of SPPs is related to the incident photons and their interactions with the nano-gratings. The energy of SPPs can be easily

**Fig. 8** The doping profile for the proposed GaAs PIN photodetector

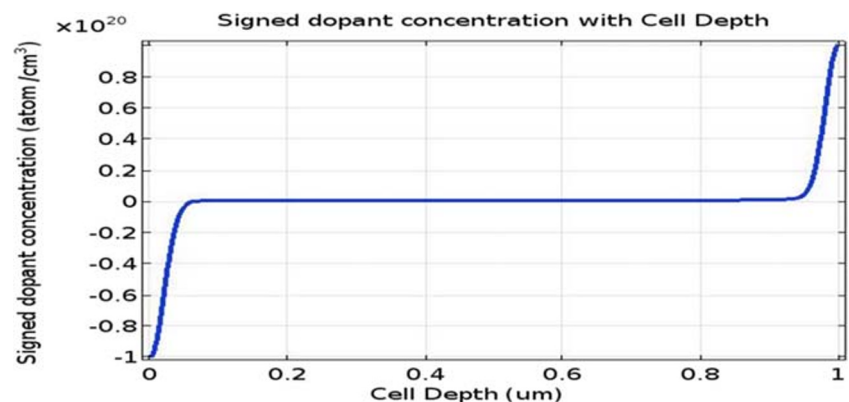
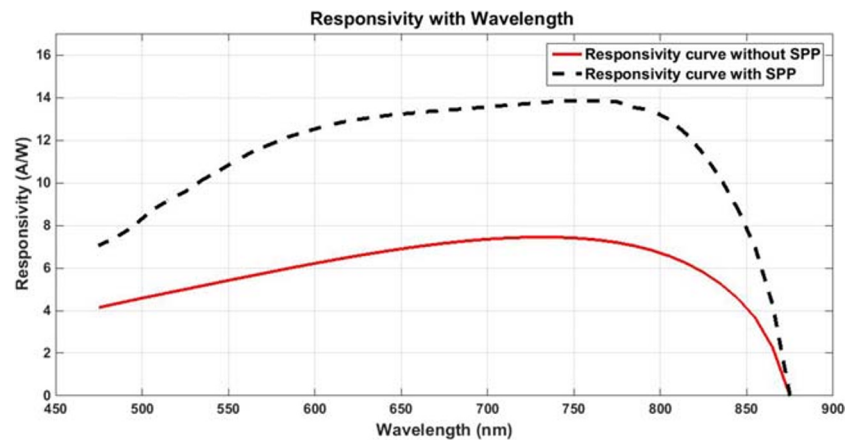


**Fig. 9** Responsivity versus wavelength for the PIN GaAs photodetector

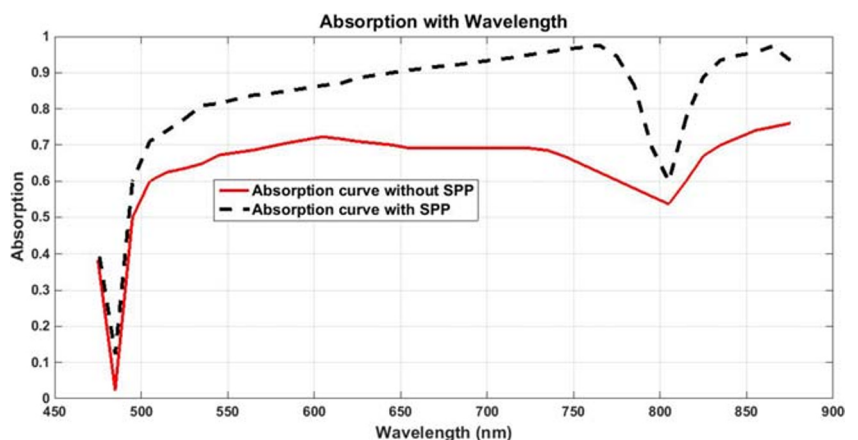


adjusted by adding thin layers of material on the metal surface or by varying the dielectric constant of the material placed on it. In periodic subwavelength structures, nano-gratings are placed on top of the underlayer from the same metal (gold). Enhanced absorption can be achieved through the SPP resonant excitations in the subwavelength domain. One method for exciting the SPPs is the nano-grating coupling technique in which the incident radiation is coupled to the SPPs using a periodic surface corrugation [43].

### Photocurrent Scan as a Function of Wavelength

For a radiant light intensity of  $1 \text{ W/cm}^2$ , the photocurrent response was computed for a wavelength range of 475–875 nm in increments of 50 nm. Several fascinating characteristics can be observed in Fig. 5. From 475 to 750 nm, the current values increase steadily with the wavelength, while jumps in current are observed at 775 nm, showing a fluctuating phenomenon. The study was restrained to 875 nm. The functional voltage boosts the photocurrent advances, demonstrating carrier trapping from the potential barriers in the GaAs structure.

**Fig. 10** Absorption versus wavelength for the PIN GaAs photodetector



### Spectral Response

One of the key results predicted from our simulation is a linear relation between the maximum value of the photocurrent and its irradiance, i.e., the radiant intensity per unit area of the detector surface. This linear relation is important in the development of electro-optical devices, and nanoscale-based sensors in particular, as it facilitates the prediction of the current produced for a given irradiance. The photocurrent in the PIN GaAs photodetector is directly proportional to the incident light intensity. This relation is clearly revealed in Fig. 6.

### Internal Quantum Efficiency

The internal quantum efficiency (IQE) of the photodetector is dependent on the absorbed optical power in the device. IQE is a key parameter for calculating the implementation of the photodetector. It is able to be described through the number of carriers that participate in the photocurrent ( $I_{ph}$ ). In our model we controlled the IQE for the functional wavelength. We observed that at 600 nm, the IQE without SPP was 42% and with SPP was 85%, an improvement of 43%. At 675 nm, the IQE without SPP was 45% and IQE with SPP was 82%,

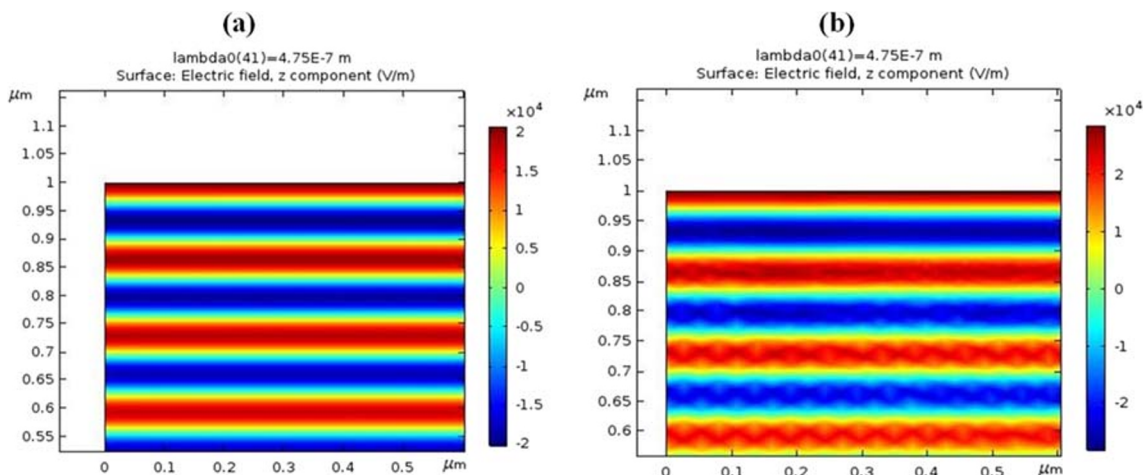


Fig. 11 Electric field intensity at the surface of the modeled PIN photodetector (a) without SPP and (b) with Au SPP

indicating an improvement of 37%. The model dimensions were tested in several iterations to obtain the best IQE. We studied different SPP layer widths with 300 nm and distance between SPP layers 700 nm, with the best IQE observed in SPP layer width with 500 nm (Fig. 7).

### Signed Dopant Concentration

Figure 8 shows the signed doping profile of the proposed model with 100 nm of P+ doping material on the surface of the model and 100 nm of N+ doping material. The absorption of photons produces both a majority and a minority carrier. In many photovoltaic applications, the number of light-generated carriers is orders of magnitude lower than the number of majority carriers already produced in the solar cell owing to doping. Therefore, the number of majority carriers in an illuminated semiconductor does not change significantly. The reverse is true, however, for the number of minority carriers. The number of photo-generated minority carriers is larger than the number of minority carriers present in the doped solar cell in the dark, because in doping, the minority carrier concentration is extremely small, and thus the number of minority

carriers in an illuminated solar cell can be estimated by the number of light-generated carriers.

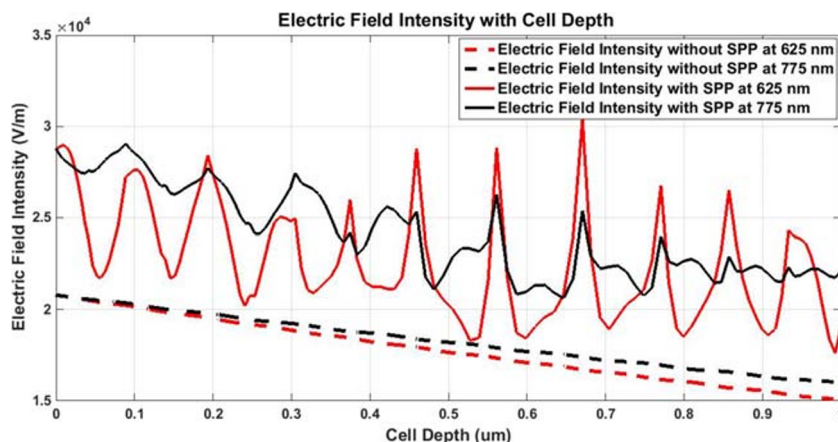
### Responsivity

One of the most fundamental parameters in assessing photodetector performance is the responsivity (R). Figure 9 shows the responsivity of the photodetector without SPP and with SPP. The results of the simulation reveal that at  $\lambda = 750$  nm, the responsivity without SPP is 7.5 A/W and with SPP is 13 A/W, which constitutes an enhancement of 5.5 A/W in our model. Additionally, at  $\lambda = 775$  nm, the responsivity without SPP is 7 A/W and with SPP is 14 A/W, resulting in a notable improvement of 7 A/W in our proposed GaAs PIN photodetector model.

### Absorption as Function of Wavelength

The absorption enhancement graph for the Au SPP photodetector is presented in Fig. 10. It can be observed that the maximum absorption improvement for the Au SPP occurs at

Fig. 12 Electric field intensity versus cell depth at the surface of the modeled PIN photodetector without SPP and with Au SPP



a wavelength of 775 nm, whereas the maximum absorption without the SPP occurs at 625 nm.

## Electric Field Intensity

The results for the simulation of electric field distribution along the  $x$  and  $y$  directions for particular structures are shown in Fig. 11. The influence of electric field intensity for a traditional PIN photodetector without the SPP just on the GaAs substrate is indicated by the cross-sectional area in Fig. 11a. For the Au SPP, the light intensity across the SPPs combining properties is noticeably observed along the aperture where the electric field intensity is maximized, as the incident light aids electrons to swap their uniqueness as plasmon polaritons with support of the Au SPP. In Fig. 12 it can be observed from the electric field intensity figure that there is an enhancement using Au SPP in the PIN photodetector at wavelengths of 775 nm and 625 nm versus without adding the SPP.

## Conclusion

In this research paper, we present a PIN photodetector with an SPP technique. In the given GaAs PIN photodetector model, we utilized gold as the SPP layer. Here, we exhibit a gold SPP photodetector attaining improvement in internal quantum efficiency (IQE) of 43%. The excellent performance is attributed to the subwavelength restraint of the optical power in a photoconductive-based gold SPP GaAs that enables high internal quantum efficiency. In addition, the arrangement of the SPP in the photodetector shows higher photocurrent and responsivity.

## Compliance with Ethical Standards

**Conflict of Interest** The authors declare no conflict of interest.

## References

1. Maier SA, Brongersma ML, Kik PG, Meltzer S, Requicha AA G, Atwater HA (2001) Plasmonics - a route to nanoscale optical devices. *Adv Mater Wiley Online Library*, Article 13(19):1501–1505
2. Atwater HA, Polman A (2010) Plasmonics for improved photovoltaic devices. *Nat Mater* 9(3):205–213
3. Schuller JA, Barnard ES, Cai WS, Jun YC, White JS, Brongersma ML (2010) Plasmonics for extreme light concentration and manipulation. *Nat Mater* 9(3):193–204
4. Gramotnev DK, Bozhevolnyi SI (2010) Plasmonics beyond the diffraction limit. *Nat Photonics* 4(2):83–91
5. Kauranen M, Zayats AV (2012) Nonlinear plasmonics. *Nat Photonics* 6(11):737–748
6. Leuthold J et al (2013) Plasmonic Communications: Light on a Wire. 24(5):28–35
7. Haffner C et al (2015) All-plasmonic Mach-Zehnder modulator enabling optical high-speed communication at the microscale. *Nat Photonics* 9(8):525–528
8. Brongersma ML (2016) Plasmonic Photodetectors, Photovoltaics, and hot-Electron devices. *Proc IEEE* 104(12):2349–2361
9. Hoessbacher C et al (2017) Optical interconnect solution with Plasmonic modulator and Ge Photodetector Array. *IEEE Photonics Technol Lett* 29(21):1760–1763
10. Brongersma ML, Halas NJ, Nordlander P (2015) Plasmon induced hot carrier science and technology. *Nat Nanotechnol* 10(1):25–34
11. Heni W et al (2016) 108 Gbit/s Plasmonic Mach-Zehnder modulator with > 70-GHz electrical bandwidth. *J Lightwave Technol Proc Paper* 34(2):393–400
12. Hoessbacher C et al (2017) Plasmonic modulator with > 170 GHz bandwidth demonstrated at 100 GBd NRZ. *Opt Express* 25(3):1762–1768
13. Mikami H, Gao L, Goda K (2016) Ultrafast optical imaging technology: principles and applications of emerging methods. *Nano Photonics* 5(4):497–509
14. Wang JQ et al (2016) High-responsivity graphene-on-silicon slot waveguide photodetectors. *Nanoscale* 8(27):13206–13211
15. Maier SA (2007) Plasmonics: fundamentals and applications. New York: Springer, Book, Chapter 2
16. Barnes WL, Dereux A, Ebbesen TW (2003) Surface plasmon sub-wavelength optics. *Nature* 424:824–830
17. Pendry JB, Martín-Moreno L, Garcia-Vidal FJ (2004) Mimicking surface plasmons with structured surfaces. *Science* 305(5685):847–848
18. Maier SA, Andrews SR, Martín-Moreno L, Garcia-Vidal FJ (2006) Terahertz surface plasmon-polariton propagation and focusing on periodically corrugated metal wires. *Phys Rev Lett* 97(17):176805
19. Gan Q, Fu Z, Ding YJ, Bartoli FJ (2008) Ultrawide-bandwidth slow-light system based on THz plasmonic graded metallic grating structures. *Phys Rev Lett* 100(25):256803
20. Li D, He J, Ding G, Tang Q, Ying Y, He (2018) Borophene: Stretch-Driven Increase in Ultrahigh Thermal Conductance of Hydrogenated Borophene and Dimensionality Crossover in Phonon Transmission. *Adv Funct Mater* 28(31):1–7
21. Tang W, Lin W, Chen X, Liu C, Yu A, Lu W (2016) Dynamic metamaterial based on the graphene split ring high-Q Fano-resonator for sensing applications. *R Soc Chem Na-oscale* 8:15196–15204
22. Lockyear MJ, Hibbins AP, Sambles JR (2009) Microwave surface-plasmon-like modes on thin metamaterials. *Phys Rev Lett* 102(7):073901
23. Okamoto T (2001) Near-field optics and surface plasmon polaritons. Springer, Topics in Applied Physics, vol 81, pp 97–122
24. Zeng, Shuwen, Yu, Xia, Law, Wing-Cheung, Zhang, Yating, Hu, Rui, Dinh, Xuan-Quyen, Ho, Ho-Pui, Yong, Ken-Tye (2013) Size dependence of Au NP-enhanced surface plasmon resonance based on differential phase measurement. *Sensors Actuators B: Chem* 176:1128–1133
25. Raether, Heinz (1988) Surface Plasmons on smooth and rough surfaces and on gratings. Springer tracts in modern physics 111. New York: Springer-Verlag. ISBN 978-3540173632
26. Cottam MG (1989) Introduction to surface and Superlattice excitations. New York: Cambridge University Press. ISBN 978-0750305884
27. Kittel C (1996) Introduction to solid state physics (8th). Hoboken: Wiley. ISBN 978-0-471-41526-8
28. Dostalek J, Ctyroky J, Homola J, Brynda E, Skalsky M, Nekvindova P, Spirkova J, Skvor J, Schrofel J (2001) Surface plasmon resonance biosensor based on integrated optical waveguide. *Sensors Actuators B Chem* 76:8–12
29. Homola J (2006) Surface Plasmon resonance based sensors. Springer series on chemical sensors and biosensors, 4. Berlin: Springer-Verlag. ISBN 978-3-540-33918-2

30. Salamin Y, Ma P, Baeuerle B, Emboras A (2018) Yuriy Myronovych Fedoryshyn, Wolfgang Heni, Bojun Cheng, Arne Josten, and Juerg Leuthold “100 GHz Plasmonic Photodetector”. *ACS Photonics* 5(8):3291–3297
31. Xuewei Zhao, Moeen M, Toprak MS, Guilei Wang, Jun Luo, Xingxing Ke, Zhihua Li, Daoqun Liu, Wenwu Wang, Chao Zhao, Radamson H (2019) Design impact on the performance of Ge PIN photodetectors. *J Mater Sci: Mater Electron* 1–8
32. Yaakov Mandelbaum, Avraham Chelly, Avi Karsenty (2018) Laser beam scanning using near-field scanning optical microscopy nanoscale silicon-based photodetector. *J Nanophotonics* 12(3): (036002(1–14))
33. Gay G, Alloschery O, Lesegno BVd, Weiner J, Lezec HJ (2006) *Phys Rev Lett* 96:213901
34. Dionne JA, Lezec HJ, Atwater HA (2006) *Nano Lett* 6:1928
35. Collin S, Fabrice P, Teissier R, Pelouard J-L (2004) *Appl Phys Lett* 85:194
36. Liu N, Mesch M, Weiss T, Hentschel M, Giessen H (2010) Infrared perfect absorber and its application as plasmonic sensor. *NanoLetters* 10(7)2342–2348
37. Abdelsalam ME, Bartlett PN, Baumberg JJ, Coyle S (2004) Preparation of arrays of isolated spherical cavities by self-assembly of polystyrene spheres on self-assembled prepatterned macroporous films. *Adv Mater* 16(1)90–93
38. Tao H, Landy NI, Bingham CM, Zhang X, Averitt RD, Padilla WJ (2008) A metamaterial absorber for the tera hertz regime: design, fabrication and characterization. *Optics Express* 16(10)7181–7188
39. Ye YQ, Jin Y, He S (2010) Omnidirectional, polarization insensitive and broadband thin absorber in the terahertz regime. *J Opt Soc Am B: Opt Phys* 27(3):498–504
40. Park H, Kim, Ho J, Beresford R, Xu J (2011) Effects of electrical contacts on the photoconductive gain of nanowire photodetectors. *Appl Phys Lett* 99(14):143110
41. Ozbay E (2006) Plasmonics: merging photonics and electronics at nanoscale dimensions. *Science* 311(5758):189–193
42. Das N, Karar A, Vasiliev M, Tan CL, Alameh K, Lee YT (2011) Analysis of Nano-grating-assisted light absorption enhancement in metal-semiconductor-metal photodetectors patterned using focused ion-beam lithography. *Opt Commun* 284(6):1694–1700
43. Gordon R, Sinton D, Kavanagh KL, Brolo AG (2008) A new generation of sensors based on extra ordinary optical transmission. *Acc Chem Res* 41(8):1049–1057

**Publisher's Note** Springer Nature remains neutral with regard to jurisdictional claims in published maps and institutional affiliations.